PFC/JA-86-12

Measurements of Amplification and Phase Shift (Wave Refractive Index) in a Free-Electron Laser

Fajans, J. and Bekefi, G.

March 1986

Plasma Fusion Center
Massachusetts Institute of Technology
Cambridge, Massachusetts 02139 USA

This work was supported in part by the National Science Foundation, in part by the Air Force Office of Scientific Research, and in part by the Hertz Foundation.

Submitted for publication to The Physics of Fluids

Measurements of Amplification and Phase Shift (Wave Refractive Index) in a Free-Electron Laser

J. Fajans and G. Bekefi
Department of Physics and Research Laboratory of Electronics
Massachusetts Institute of Technology
Cambridge, Massachusetts 02139

Abstract

Measurements of the amplification and phase shifts (wave refractive index) in a free electron laser are reported. The studies have been carried out at microwave frequencies (7-16GHz) in a free electron laser operating in the collective (Raman) regime, using a mildly relativistic electron beam with energy of $\sim$ 160keV, and current of $\sim$ 5A. The observations are found to be in excellent agreement with theoretical predictions based on the full three dimensional FEL dispersion relation.

This work was supported in part by the National Science Foundation, in part by the Air Force Office of Scientific Research, and in part by the Hertz Foundation.

I Introduction

The collective (Raman) free electron laser (FEL) produces coherent radiation by subjecting a cold intense electron beam to a transverse, periodic "wiggler" magnetic field that induces transverse oscillations on the electron beam. The undulating electron beam interacts with an incident electromagnetic wave to produce an axially directed ponderomotive force.[1,2] This force causes axial bunching of the undulating electron beam, thereby driving the incident electromagnetic wave. The energy for the radiation comes at the expense of the beam kinetic energy.

In a previous study[3,4] we focussed our attention on the frequency characteristics of the emitted radiation, and the effects of the electron dynamics on the emission properties. We demonstrated continuous FEL tuning with beam energy from 7-21GHz, observed output powers in excess of 1MW, and found that as much as 12% of the electron beam energy can be converted into coherent electromagnetic radiation in a single (TE_{11}) waveguide mode. Reference 4 also contains an extensive listing of experimental work in other laboratories.

The present work concerns two other major aspects of free electron lasers. One is wave amplification (proportional to the imaginary part of the FEL dispersion characteristics) which we have studied as a function of various parameters including frequency, the strength of the wiggler magnetic field, the strength of the guide magnetic field, electron beam current, energy and temperature, and axial distance within the interaction region.

The other aspect concerns the phase shifts and wave refractive index associated with the FEL dispersion characteristic. The behavior of the real part of the dispersion relation is critical to the theoretically predicted phenomena of optical guiding,[5] in which the electromagnetic radiation energy is guided by the electron beam in a fashion similar to light being guided on an optical fiber. Optical guiding is thought to be necessary in future high frequency FELs to extend the interaction length beyond the Rayleigh range. Our measurements provide

the first experimental masurement of FEL induced shifts in the real part of the dispersion relation, (albeit in a frequency range far different from that of interest to optical guiding).

In comparing experiment with theory we find it necessary to use the full, spatially dependent,[6] dispersion equations discussed below which take cognizance of initial conditions,[7] and the interference between all of the active and passive waves. In general, excellent agreement is found between measurements and theory.

II —Theoretical Considerations

The free electron laser can be analyzed[1,2] as an interaction between three waves; a guided electromagnetic wave with dispersion relation

$$\omega^2 = c^2k^2 + w_c^2 \tag{1}$$

and two space charge waves

$$\omega = (k + k_w)\beta_\| c = p_1\omega_p\Phi^{1/2}/\gamma_\|\gamma^{1/2}, \tag{2}$$

where the plus sign corresponds to the fast positive energy, "passive" space charge wave, and the minus sign corresponds to the slow, negative energy, "active" space charge wave. Here ω and k are the interaction frequency and wavenumber, $\omega_c^2 = \omega_{c0}^2 + p_2\omega_p^2/\gamma$ is the effective waveguide cutoff frequency adjusted for the presence of the electron beam, ω_{c0} is the empty waveguide cutoff frequency (in our case the lowest mode of a circular waveguide (TE_{11}); $k_w = 2\pi/l$ is the wiggler wavenumber, $\beta_\| = v_\|/c$ is the normalized axial velocity of the electron beam, $\omega_p = (Ne^2/m_0\epsilon_0)^{1/2}$ is the nonrelativistic plasma frequency, $\gamma_\|^2 = 1/(1 - \beta_\|^2)$ is the Lorentz contraction factor. The relativistic mass increase $\gamma = 1 + eV/m_0c^2$ measures the beam energy, Φ is the adjustment to the plasma frequency due to the combined wiggler and axial magnetic fields, p_1 is the reduction to the plasma frequency that results from finite radius effects,[8] and p_2 is the electromagnetic wave energy weighted ratio of the electron beam cross-section and the waveguide area. In normal operation of our FEL, $p_2 \approx 0.06$ so that $\omega_c \approx \omega_{c0}$, $p_1 \approx 0.5$, and $\Phi \approx 1$.

The FEL operation is usually centered around the frequency at which the electromagnetic wave and the slow space charge wave are in phase synchronism, which occurs near the radiation frequency.

$$\omega = \beta_{\|} c k_{w,\mathrm{eff}} \gamma_{\|}^2 \left\{ 1 \pm \beta_{\|} \left[1 - \left(\frac{w_c}{k_{w,\mathrm{eff}} \gamma_{\|} \beta_{\|}} \right)^2 \right]^{1/2} \right\} \tag{3}$$

where the effective wiggler wavenumber $k_{w,\mathrm{eff}} = k_w - p_1 \omega_p \Phi^{1/2} / \gamma_{\|} \gamma^{1/2} \beta_{\|} c$ and the $\pm$ sign selects the high and low frequency branches of the FEL instability. The lower frequency branch leads to radiation at the frequency near the cutoff frequency and will henceforth be of no further interest to this paper (measurements at the lower frequency branch are discussed in Refs. 3 and 4). The high frequency branch, $\omega \approx \beta_{\|} c k_{w,\mathrm{eff}} \gamma_{\|}^2 (1 + \beta_{\|})$ exhibits the well-known $\gamma_{\|}^2$ upshift.

The FEL gain G, defined as the ratio of the output power $P(z)$ at a distance z within the interaction region to the total input power $P(0)$ injected at position $z = 0$. is given by the relation[7]

$$G = \frac{P(z)}{P(0)} = \left| \frac{a(z)}{a(0)} \right|^2 \tag{4}$$

where $a(z)/a(0)$ is the ratio of the electric field amplitudes

$$\frac{a(z)}{a(0)} = \sum_j A_j e^{i k_j z} \tag{5}$$

summed over all the interacting waves j. A_j is the normalized wave amplitude of a given wave and k_j is the associated complex propagation constant; the k_j can result in wave growth ($\mathrm{Im}\ k_j < 0$), damping ($\mathrm{Im}\ k_j > 0$), or in a passive wave ($\mathrm{Im}\ k_j = 0$). The numerical values of $k_j \equiv k + \delta k_j$ and A_j are determined from the poles and residue, respectively, of the relation[7]

$$A(\delta k) = \frac{(\delta k - \theta + \theta_p)(\delta k - \theta - \theta_p)}{\delta k (\delta k - \theta + \theta_p)(\delta k - \theta - \theta_p) + Q}, \tag{6}$$

where k is the wavenumber of the unperturbed electromagnetic wave as determined from Eq. (1). and $\theta_p = p_1 \omega_p \Phi^{1/2} / \gamma_{\|} \gamma^{1/2} \beta_{\|} c$ is the normalized plasma frequency associated with the electron beam; $\theta = \omega / \beta_{\|} c - k - k_w$ is the "detuning parameter" which determines the FEL operating point; ($\theta = -\theta_p$ corresponds to the situation

given by Eq. (3)). Finally, the quantity Q is a measure of the interaction strength and is defined as[7]

$$Q = p_2 F \beta_{\perp}^2 k_w^2 \gamma_{\parallel}^4 \theta_p^2 (1 + \beta_{\parallel})^2 / 4 k p_1^2 \tag{7}$$

Here $\beta_{\perp} = v_{\perp}/c$ with $v_{\perp}$ as the amplitude of the transverse velocity acquired by the electron in the applied wiggler magnetic field. The finite radial extent of the electron beam and the transverse mode structure require several correction to the standard one dimensional value of the interaction strength. Most of these corrections can be successfully modeled by appropriately calculating p_1 and p_2. The parameter $F \approx 1$ contains the detailed three dimensional corrections, and is derived from the theoretical work of Freund and Ganguly.[6] Unfortunately, it is not readily written in closed form. In the collective (Raman) regime of our experiment, maximum gain occurs when the detuning parameter θ equals $-\theta_p$. Under these conditions, k of Eq. (6) becomes

$$\delta k = i\sqrt{Q/2\theta_p} = \pm i \frac{1}{2\sqrt{2}} \beta_{\perp} k_w (1 + \beta_{\parallel}) \gamma_{\parallel}^2 \left[\frac{p_2 F \omega_p}{p_1 k \gamma_{\parallel} \gamma^{1/2} \beta_{\parallel} c^2} \Phi^{1/2} \right]^{1/2} \equiv \pm \Gamma \tag{8}$$

where Γ defines the growth (or damping) rate. Moreover, examination of the residues of Eq. (6) shows that the amplitude of the injected wave splits equally between the exponentially growing mode and the exponentially damped mode, with the result that Eq. (4) becomes

$$P_{\text{out}}/P_{\text{in}} = \left[\frac{1}{2} \exp(\Gamma z) + \frac{1}{2} \exp(-\Gamma z) \right]^2 = \cosh^2(\Gamma z). \tag{9}$$

Thus, we see that only one quarter of the injected power goes into the amplified wave and represents a 6dB "launching loss". We note that FEL's with helical wigglers (as in our case), amplify circularly polarized waves. Injection and detection of a linearly polarized wave causes additional loss, since the linearly polarized wave decomposes into two waves with only one having the correct "handedness". It is readily shown that Eq. (9) becomes

$$P_{\text{out}}/P_{\text{in}} = \left[\frac{1}{4} \exp(\Gamma z) + \frac{1}{4} \exp(-\Gamma z) + \frac{1}{2} \right]^2 = [\cosh(\Gamma z) + 1]^2/4. \tag{10}$$

The overall launching loss is now 12dB.

Equations 4 through 6 also contain complete information concerning the phase shifts and wave refractive index associated with the FEL interaction, which are contained in the quantity

$$(\Delta k)z = \tan^{-1}\left[\frac{\mathrm{Im}\left(\sum_j A_j e^{ik_j z}\right)}{\mathrm{Re}\left(\sum_j A_j e^{ik_j z}\right)}\right] \tag{11}$$

where $(\Delta k)z$ represents the phase slippage (or phase advance) relative to the phase of the unperturbed electromagnetic wave. We may then define the wave refractive index μ as

$$\mu - 1 = (c/\omega)\Delta k. \tag{12}$$

The above expressions show that the FEL gain and refractive index are critically dependent on accurate knowledge of the electron axial velocity $\beta_\parallel$ and tranverse velocity $\beta_\perp$ in the combined guide and wiggler magnetic fields, which in cylindrical coordinates (r, ϕ, z) are given by[9]

$$\begin{aligned}\mathbf{B} = \hat{\mathbf{e}}_z B_\parallel + 2B_w\Big(&\hat{\mathbf{e}}_r I_1'(k_w r)\cos(\phi - k_w z) - \hat{\mathbf{e}}_\phi \frac{I_1(k_w r)}{k_w r}\sin(\phi - k_w z) \\ &- \hat{\mathbf{e}}_z I_1(k_w r)\sin(\phi - k_w z)\Big)\end{aligned} \tag{13}$$

Here I_1 is the modified Bessel function. Recent calculations and computer simulations have shown that despite the complicated three dimensional nature of the magnetic field, electrons launched into a wiggler with a gradually rising (adiabatic) entrance field travel at nearly constant axial velocity $\beta_\parallel$, and acquire a transverse velocity given by an equation for the electrons perpendicular velocity[10]

$$\beta_\perp = \frac{2\Omega_w \beta_\parallel I_0(k_w y_g) I_1(\lambda)/\lambda}{k_w \beta_\parallel c - \Omega_\parallel - 2\Omega_w I_0(k_w y_g) I_1(\lambda)} \tag{14}$$

where $\Omega_w = eB_w/\gamma mc$ is the relativistic cyclotron frequency associated with the wiggler magnetic field, $\Omega_\parallel = eB_\parallel/\gamma mc$ is the relativistic cyclotron frequency of the axial field, y_g is the distance of the electron guiding center from the wiggler axis, and $\lambda = \beta_\perp/\beta_\parallel = \pm k_w r$ is the normalized size of the orbit, such that $\lambda = -k_w r$ when $\Omega_\parallel > k_w \beta_\parallel c$ and $\lambda = +k_w r$ when $\Omega_\parallel < k_w \beta_\parallel c$. However, for the parameters of this experiment, $I_0(k_w y_g)$ is 1.008. Consequently the above expression can be simplied to read[10,11]

$$\beta_\perp = \frac{2\Omega_w \beta_\parallel I_1(\lambda)/\lambda}{k_w \beta_\parallel c - \Omega_\parallel - 2\Omega_w I_1(\lambda)} \tag{15}$$

which is the form used in our calculations. Finally, to obtain $\beta_{\|}$, Eq. (15) must be solved together with the energy conservation equation $1/\gamma^2 = 1 - \beta_{\|}^2 - \beta_{\perp}^2$.

In the presence of an axial guide magnetic field, FEL operation can be divided into two main regions depending on whether $\Omega_{\|}$ is smaller or greater than $k_w\beta_{\|}c$. In most (but not all) of the experiments discussed below the axial magnetic field $B_{\|}$ is sufficiently weak so that $\Omega_{\|} < k_w\beta_{\|}c$. In this situation the electrons are in the so-called Group I orbits and are not dramatically perturbed by the axial field.

III—Experimental Apparatus

A schematic of the FEL is shown in Fig. 1. More details of the experimental arrangement are given in Refs. 4 and 12. The accelerating potential for the laser is supplied by a Marx generator (Physics International Pulserad 615MR, which has a maximum capability of 500kV and 4kA). Since the accelerator does not use a pulseforming network, the output voltage pulse is essentially that of a discharging capacitor bank ($C = 0.083\mu$F) with a shunt adjusted RC time constant of $10 - 100\mu$s. The output voltage is monitored by a carefully calibrated resistive divider network. (The calibration error is estimated to be less than two percent.) Because the FEL's properties depend strongly on the exact knowledge of the electron beam voltage, the noise-free voltage pulse produced by the 615MR proves to be very important in data acquisition and data interpretation.

The electron beam is generated by a thermionically emitting, electrostatically focused, Pierce-type electron gun (250kV, 250A) removed from a SLAC klystron (model 343). An assembly of six focusing coils is designed so that their magnetic field lines lie along the zero-magnetic-field electron trajectories. This field configuration gives the least scalloping of the electron beam (low transverse temperature) and allows the magnetic field amplitude to be varied over a wide range without greatly affecting the electron beam temperature. To insure good electron orbits, an aperture is inserted which limits the electron beam radius to $r_b = 0.254$cm so that only the inner portion of the beam is used. With this

precaution, previously described experiments[4] indicate that the energy spread of the beam entering the magnetic wiggler is less than $\Delta\gamma_{||}/\gamma_{||} = 0.003$.

The gun focusing coils guide the electron beam into a 2.54cm ID stainless steel evacuated drift tube. The beam is contained by a uniform axial magnetic field $B_{||}$ that has a power supply limited maximum of 7kG, and a minimum of approximately 800G. Below this value beam defocussing and deterioration occur. The current is measured before the wiggler by a Rogowski coil that is calibrated to an accuracy of five percent. In certain studies it is desirable to change the current density. This is accomplished by lowering the cathode heater current and thereby operating the gun in the temperature limited regime rather than in the space charge limited regime. The net current entering the magnetic wiggler can thus be varied from 0.1—8A.

The 50 period circularly polarized magnetic wiggler has a period $l = 3.3\text{cm}(k_w = 2\pi/l = 1.90\text{cm}^{-1})$, a maximum amplitude $B_w = 1.5\text{kG}$, and is generated by bifilar conductors[13-15] wound directly on the outside of the stainless steel drift tube. Since the beam aperture limits the size of the beam to $k_w r_b \approx 0.5$, the wiggler field is close to that of an ideal wiggler. That is, the effects of the radial variation of the wiggler field and the presence of the off-axis components are usually small. At the wiggler entrance a slowly increasing field amplitude is produced by resistively loading the first six periods of the wiggler magnet.[16]

The 2 meter long 2.45cm ID drift tube acts as a cylindrical waveguide whose fundamental TE_{11} mode has a cutoff frequency of $\omega_{c0}/2\pi = 6.92\text{GHz}$. The stainless steel drift tube is copper plated (thickness 0.3mils) to decrease attenuation. Microwaves are launched onto the electron beam by a carefully designed TE_{10} rectangular guide to TE_{11} circular wave guide coupler (see Fig. 1). The coupler incorporates an E-plane miter bend with a small hole in the waveguide wall for the electron beam, so that the microwaves can be launched colinearly with the beam. The coupler characteristics are fairly flat within the $\sim 7 - 17\text{GHz}$ frequency range of the experiments reported in this paper.

At the output end of the wiggler a mica vacuum window transmits the circularly polarized FEL radiation propagating in the drift tube into a broadband circular guide to a rectangular guide transformer, which couples the FEL emission out of the system in the form of a linearly polarized wave traveling in the rectangular guide. Thus, all the FEL characteristics, including gain, spectral and phase measurements are measured using standard, rectangular waveguide components.

IV—Measurements of Rf Power and Gain

Figure 2 illustrates a typical amplifier shot. Since the accelerator has an RC droop (as discussed in section III) the beam energy sweeps through a range of values as seen in Fig. 2a. Amplification occurs (Fig. 2b) at the time during voltage pulse when the voltage reaches the appropriate value as predicted by Eq. (3). In addition to wave growth, one also observes wave absorption in which energy from the wave is converted into kinetic energy of the electrons. This wave absorption is attributed to an interaction with the fast space charge wave (see section II).

To assures ourselves that proper amplification does in fact occur, the RF output power is measured as a function of the RF input power, as is illustrated in Fig. 3. We see that the FEL gain (ratio of power out to power in) is constant over an 80dB range of input signals. (Saturation observed at input power levels in excess of $\sim$ 1kW will be discussed in a later paper.)

4.1. Gain as a Function of Wiggler Field Amplitude.

The measurement of gain as a function of wiggler strength B_w is shown in Fig. 4 under conditions of constant input frequency, beam current and axial guide field $B_{||}$. The RF input power is less than 10W. To factor out the effect of the waveguide attenuation, the gain is here defined as the ratio of the amplified power $P_{\rm out}$ to the power $P_{\rm out}$ when the electron beam is not present. Because of spontaneous oscillations, gains greater than 20dB cannot be measured.

The experiments shown by solid dots are in good agreement with three dimensional theory for the gain [Eqs. (8), (10)] which takes into account the finite

radial extent of the electron beam, the radial field variations of the TE_{11} waveguide mode, and of the wiggler field strength, as discussed in section II. It is important to note that for low gains ($P_{out}/P_{in} \simeq 1$), "launching losses" are important and must be allowed for in calculating the gain in conformity with Eq. (10).

4.2. Gain as a Function of Axial Distance

In order to measure the FEL gain as a function of the axial distance z, the electron beam is prevented from traversing the entire 165cm length of the magnetic wiggler. This is accomplished by means of an axially movable horseshoe "kicker" magnet which deflects the beam into the waveguide wall at any desired postion z, thereby terminating the FEL interaction at that point.

Figure 5 illustrates the experimental results. The squares represent the measured gain, and the dashed line is from three dimensional theory based on Eqs. (8) and (10). The growth rate Γz can be unfolded from the measured gain by use of Eq. (10). The results are represented in Fig. 5 by the solid points. The solid line is from Eq. (8). We see that the growth rate Γz increases linearly with distance z, in accordance with expectations. However, for stronger axial wiggler fields and input powers than those used here the gain eventually levels off due to nonlinear saturation, as will be discussed in a later publication.

4.3. Gain as a Function of Frequency

Figure 6 illustrates how the FEL gain varies with frequency ω of the input signal, at constant axial magnetic field $B_{\|}$ = 1580G and two values of wiggler field, B_w = 130G and 168G. The gain shown plotted is the maximum gain corresponding to the resonant electron beam energy for which the detuning parameter θ equals $-\theta_f$ (see section II). The agreement between measurements and predictions from Eqs. (8) and (10) are satisfactory. In making this comparison cognizance is taken of the fact that as ω and the wiggler field B_w are varied,, the beam energy γ and the electron beam current I also vary. Typically, I changes from $\sim$ 3.5A at low beam energies and wiggler fields to $\sim$ 8.4A at higher beam energies and

wiggler fields. This variation is taken into account in calculating the theoretical gain curves of Fig. 6.

The strong peak in the gain at a frequency of $\sim$ 8.5GHz occurs near the merging of the high and low frequency branches of the FEL instability, corresponding to the critical frequency $\omega \approx \beta_{\|} c k_{w,\mathrm{eff}} \gamma_{\|}^2 = \gamma_{\|} \omega_c$ of Eq. (3). Thus the peak occurs at the threshold energy below which no FEL interaction can take place for the given fixed set of parameters, ω_c and $k_{w,\mathrm{eff}}$. At this critical frequency the growth rate Γ of Eq. (8) is the highest due to the three effects. First, $\gamma_{\|}$ and $\beta_{\|}$ are as low as they can be; secondly $\beta_{\perp}$ for group I orbits is highest when the beam energy is low, as is found by solving the orbit equation (14); and thirdly, the plasma frequency reduction factor p_1 is lower at lower frequencies. All these effects increase the gain (see Eq. (8)).

4.4. Gain as a function of Beam Current

In the Raman regime the growth rate Γ is proportional to the square root of the plasma frequency, and thus to the fourth root of the electron beam current I. In Fig. 7a, the measured gain is shown as a function of the beam current for a frequency of 11.25GHz, a wiggler field B_w = 170G, and an axial field $B_{\|}$ = 1580G. The beam current is varied by changing the cathode temperature. For currents above 0.3A the gain is in excellent agreement with Eqs. (8) and (10) appropriate to the cold beam, Raman FEL theory; but below $\sim$ 0.3A the gain falls much faster than predicted by the Raman theory. The discrepancy is more obvious when the growth rate Γ divided by the fourth root of the current is plotted as a function of the current (Fig. 7b). The growth rate Γ is constructed from the measured gain G by use of Eq. (10). We see that $\Gamma/I^{1/4}$ is approximately constant above a beam current of 0.3A, but below this current $\Gamma/I^{1/4}$ falls very quickly, and the experiment enters the region generally referred to as the "weak pump, warm beam Compton regime".

The rapid decrease in gain at low currents below that predicted by Raman FEL theory observed in Fig. 7 is due to Landau damping of the slow space charge

wave. As seen from Eq. (2) the lower the value of ω_p the higher the phase velocity $v_p = \omega/k$ of the slow space charge wave. When v_p approaches the electron thermal velocity, strong Landau damping sets in and causes a reduction of the FEL gain.

The quantitative decrease in the gain can be found by modifying Eq. (6) to read

$$A(\delta k) = \frac{(\delta k - \theta + \theta_p + i\theta_t)(\delta k - \theta - \theta_p + i\theta_t)}{\delta k(\delta k - \theta + \theta_p + i\theta_t)(\delta k - \theta - \theta_p + i\theta_t) + Q}, \tag{16}$$

where the normalized Landau damping rate θ_t is defined as[17]

$$\theta_t = \sqrt{8\pi}\frac{\omega}{\gamma_{\|}^2\beta_{\|}^3 c}\frac{\Delta\gamma_{\|}}{\gamma_{\|}}\left(\frac{\Omega}{\Delta}\right)^4 \exp\left(-\frac{2\Omega^2}{\Delta^2}\right) \tag{17}$$

with $\Omega = p_1 w_p \gamma_{\|}/\omega\gamma^{1/2}$, and $\Delta = (1/\gamma_{\|}^2\beta_{\|}^2)\Delta\gamma_{\|}/\gamma_{\|}$. The dashed curves of Fig. 8b are computed from Eqs. (16) and (17) for two values of $\Delta\gamma_{\|}/\gamma_{\|}$. The assumed value of $\Delta\gamma_{\|}/\gamma_{\|} = 0.0036$ is found to agree well with the experimental data. This energy spread is slightly larger than the previously quoted maximum spread of $\Delta\gamma_{\|}/\gamma_{\|} = 0.0030$.[4] Other temperature effects will be discussed in a later paper.

4.5. Gain as a Function of Axial Magnetic Field $B_{\|}$

The studies described in the above subsections were carried in a weak axial guide magnetic field, well below resonance, such that $\Omega_{\|} < k_w\beta_{\|}c$. In this regime, the experimental observations invariably agree well with theory based on Eqs. (8) and (10). This is illustrated in Fig. 8 in which the gain is plotted as a function of $B_{\|}$. We see however, that in strong guide fields, $\Omega_{\|} \gg k_w\beta_{\|}c$, the agreement is poor for reasons that are not understood at this time.

The regime $\Omega_{\|} > k_w\beta_{\|}c$ can be further subdivided into a region close to the axial resonance where the space charge parameter Φ of section II is less than zero, and a region further removed from resonance where Φ is greater than zero. The results shown in Fig. 8 correspond throughout to the region $\Phi > 0$ and thus differences between theory and experiment illustrated there cannot be blamed on some pathological FEL behavior caused by negative values of Φ.

A lengthy effort was made to obtain gain measurements in the Φ negative region that exists very close to resonance. In this regime the FEL is found to be extremely noisy and unrepeatable, and quantitative gain measurements could not be obtained. Moreover, calculations show that launching losses in this regime can be much larger than in other regimes. In view of this, and the proximity of the cyclotron maser instability,[18,19] a very thorough experimental and theoretical study of FEL operation near resonance needs yet to be undertaken.

V—Output Polarization

By rotating the rectangular output microwave components around the circular waveguide axis, different output polarizations can be sampled. When there is no FEL interaction (i.e. when the wiggler field is zero), all of the microwaves propagating out of the system are obviously in the incident polarization, and there is no energy in the orthogonal polarization. When the FEL interaction is very strong, however, the output radiation is predominantly circularly polarized and the energies in the incident and orthogonal polarizations are nearly equal. Here the incident polarization is defined to be the polarization direction parallel to the linearly polarized microwaves sent into the system by the microwave launcher, and the orthogonal polarization is defined to be the polarization perpendicular to the initially launched wave. The ratio of the power in the two polarizations is given by

$$R = \frac{P_{\text{orthogonal}}}{P_{\text{incident}}} = \left[\frac{\cosh(\Gamma z) - 1}{\cosh(\Gamma z) + 1}\right]^2 \tag{18}$$

This ratio was measured experimentally (frequency 9GHz, beam current approximately 5.7A, and axial field strength of 1580G) as a function of the interaction strength which is varied by changing the wiggler field from 0 to 300G (see Fig. 9). Reasonable agreement is found between the theoretically predicted power ratio and the experimental measurements.

VI--Fast wave interaction

The fast wave FEL interaction at $\theta = \theta_p$ causes a shift in the real part of the radiation wavenumber (Eq. 6). Thus, unlike the slow wave interaction (at

$\theta = \theta_p$) which results in exponential growth or damping, the fast wave interaction results in interference phenomena. However, just as in the slow wave case, the initial conditions cause the input power to be split equally into two waves, one wave with a positive shift in the real part of k, and one with a negative real part shift. Since the fast wave interacts with a circularly polarized wave, the linearly polarized input power is further split into an interacting right hand wave and a noninteracting left hand wave. Consequently the output power observed in the polarization parallel to the incident input wave is

$$\frac{P_{\text{out}}}{P_{\text{in}}} = \frac{1}{4}\left[1 + \cos(\delta k z)\right]^2 \tag{19}$$

and the power observed in the orthogonal polarization is

$$\frac{P_{\text{out}}}{P_{\text{in}}} = \frac{1}{4}\left[1 - \cos(\delta k z)\right]^2 \tag{20}$$

Varying the interaction strength δk by changing the wiggler field B_w results in the interference curves shown in Fig. 10. Here the input frequency is 10.4GHz, the beam current is approximately 2.5A, and the axial field is $B_{\|} = 1422$G. The measurements are taken at the experimentally determined beam voltage that maximizes the fast wave interaction, which is a function of the wiggler strength. The data exhibit the expected sinusoidal dependence.

VII—Phase Shift and Gain Bandwidth Measurements

In the collective (Raman) regime maximum gain occurs when the detuning parameter $\theta = -\theta_p$. This corresponds to the interaction between the slow space charge wave and the electromagnetic wave (see section II). Similarly, maximum wave absorption occurs when $\theta = +\theta_p$ and corresponds to the interaction between the fast space charge wave and the electromagnetic wave. The large peak and the large dip seen in Fig. 2b correspond precisely to these two situations. We also note that at these two points (and these two points only) the total phase change (see Eq. (11)) associated with the FEL interaction is very close to zero. Thus here the wave refractive index μ of Eq. (12) is unity.

At electron beam energies for which $\theta \neq \pm\theta_p$ the situation is entirely different. Now all three waves interact simultaneously, which leads to constructive

(or destructive) wave interference between the three waves as already pointed out in Section VI. Moreover, $(\Delta k)z$ and $(\mu - 1)$ are no longer zero. Figure 11 illustrates the experimental results and comparison with theory based on Eqs. (5) through (10). Figure 11a shows a plot of the gain (or loss) as a function of the normalized beam voltage or energy. This "energy bandwidth" can be related to the customary frequency bandwidth by means of the detuning parameter. The agreement between observations and theory is seen to be very good. The fine structure between the large peak (gain) and the large dip (absorption) is due to the aforementioned wave interference. This effect can be substantial. For example, the region between the two arrows in Fig. 11 is the only region where any of the wavenumbers are imaginary, i.e. the only region where exponential gain exists. The apparent gain observed outside this region is solely due to interference between the several waves.

To determine the phase shift, $(\Delta k)z$, associated with the FEL interaction, we use a microwave interferometer technique. The RF signal from the FEL is mixed with a reference signal from the same coherent source (klystron or magnetron) which provides the input power into the FEL interaction region (see Fig. 1). The reference arm of the interferometer contains a calibrated phase shifter and an attenuator. The two signals are then mixed and rectified in a balanced crystal mixer, and the output is displayed on a fast oscilloscope. The phase is determined every 5° on a shot-to-shot basis by adjusting the phase shifter and attenuator located in the reference arm. The results of combining 10-20 successive shots allow one to determine directly the phase of the output signal that undergoes FEL interaction relative to the phase of the output signal when the FEL is turned off (vacuum case). The background phase shift due to the Faraday rotation in the electron beam is subtracted from the measurements. The results are illustrated by the solid curve of Fig. 11b, and they are in good agreement with theoretical predictions (dashed curve). Note that the maximum phase shifts occur near points of maximum gain and maximum attenuation (see Fig. 11a). However, right at those points the phase shift is close to zero in accordance with theoretical predictions. We note that the phase behavior of an FEL operating in the collective

(Raman) regime is very different from the phase behavior when the FEL operates in the single particle (Compton) regime. In the latter case, for example, the phase change is largest at maximum gain.

Figure 12 shows a series of phase and gain measurements as a function of electron beam energy, corresponding to four distinct regions of FEL operation. In order to exhibit the differences more clearly, the FEL parameters were adjusted so as to produce the same FEL gain throughout. In Fig. 12a the wiggler field is relatively low, $B_w = 73$G, and the beam current is high ($I = 5.0$A). Consequently the slow and fast space charge waves are well-separated and the curves are very similar to those shown in Fig. 11. The beam current in Fig. 12b was reduced to $I = 0.94$A, and to maintain the same overall gain, the wiggler field was increased to $B_w = 119$G. Now the slow and fast wave peaks are much closer, but are still distinct. In Fig. 12c the wiggler field was further increased to $B_w = 260$G at about the same current $I = 0.84$A and the effective wiggler length was decreased to 57cm from 152cm to maintain the same gain. The high wiggler field causes the region over which exponential gain occurs to broaden substantially; consequently the slow and fast wave regions are now contiguous. In the last case (Fig. 12d) the beam current was reduced to $I = 0.16$A where temperature effects are important. The full length 152cm wiggler was used, at a wiggler field of 260G. Here theory was fitted to the data with an assumed energy spread $\Delta\gamma_{||}/\gamma_{||} = 0.0044$ as described in section 4.4. In the last regime the operation approaches that of a single particle (Compton) FEL in the so-called low gain warm beam regime.

XII— Conclusions

In this paper we have reported on a detailed study of the amplification and phase characteristics of a free electron laser operating in the collective (Raman) regime, at electron beam energies of $\sim$ 160KeV and electron currents $\sim$ 1to5A. We believe that measurements of the FEL phase characteristics have not been previously published, and that such measurements are relevant to problems of optical guiding.[5]

The device operates reliably and reproducibly over a wide range of system parameters. The experimental observations are sufficiently precise that they allow one to distinguish between different theoretical models and approximations. For example, three dimensional effects can readily be observed. These effects include shifts in the resonant frequency and changes in the gain caused by the transverse structure of the waveguide and space charge modes. Secondly, when the gain is low and when information on launching losses, polarization of the radiation, wave interference and FEL phase are required, we find that it is necessary to use theoretical treatments based on Laplace transforms. This technique provides an appropriate vehicle for treating the initial conditions. Thirdly we find that whereas most gain calculation available in the literature are equivalent at the basic FEL resonance frequency $\omega = k_w \beta_{\|} c(1 + \beta_{\|})\gamma_{\|}^2$, they differ significantly away from this frequency, and predict different gain bandwidths. We find that our measurements agree best with Eq. (7), based on the work of reference 7.

In summary, the linear behavior of the collective (Raman) FEL has been carefully studied, and is well understood. Experience with our FEL indicates that this source, originally conceived by Motz[20] and Phillips[21], can be developed into a useful and practical source of coherent electromagnetic radiation.

References

[1]N. M. Kroll, and W. A. McMullin, *Phys. Rev. A.* **17**, 300 (1978).

[2]P. Sprangle, R. A. Smith, and V. L. Granatstein, ***Infrared and Millimeter Waves,*** K. J. Button, ed. Vol. 1, Academic Press, N.Y., 279 (1979), and references therein.

[3]J. Fajans, G. Bekefi, Y. Z. Yin, and B. Lax, *Phys. Rev. Lett.* **53**, 246 (1984).

[4]J. Fajans, G. Bekefi, Y. Z. Yin, and B. Lax, *Phys. Fluids.* **26**, 1995 (1985).

[5]E. T. Scharleman, A. M. Sessler, and J. S. Wurtele, *Phys. Rev. Lett.* **54**, 1925 (1985).

[6]H. P. Freund and A. K. Ganguly, *Phys. Rev. A.* **28**, 3438 (1983).

[7]A. Gover and P. Sprangle, *IEEE J. Quant. Elect.* **QE-17**, 1196 (1981), also E. Jerby and A. Gover, *IEEE J. Quant. Elect.* **QE-21**, 1041 (1985).

[8]G. M. Branch, and T. G. Mihran, *IRE Trans. Elect. Dev.* **ED-2**, 3 (1955).

[9]P. Diament, *Phys. Rev. A.* **23**, 2537 (1981).

[10]J. Fajans, D. A. Kirkpatrick, G. Bekefi, *Phys. Rev. A.* **32**, 3448 (1985).

[11]H. P. Freund, S. Johnston, P. Sprangle, *IEEE J. Quant. Elect.* **QE-19**, 322 (1983).

[12]J. Fajans, , Ph.D thesis, Dept. of Physics, Massachusetts Institute of Technology, Boston, (1985), (unpublished).

[13]H. Poritsky, *J. Appl. Phys.* **30**, 1828 (1959).

[14]B. Kincaid, *J. Appl. Phys.* **48**, 2684 (1977).

[15]J. R. Blewett, R. Chasman, *J. Appl. Phys.* **48**, 2692 (1977).

[16]J. Fajans, *J. Appl. Phys.* **55**, 43 (1984).

[17]W. McMullin, , Ph.D thesis, Dept. of Physics, University of California, San Diego, (1980), (unpublished).

[18]R. E. Shefer and G. Bekefi, *Int. J. Electronics.* **51**, 569 (1981).

[19]G. Bekefi and J. Fajans, *Phys. Fluids.* **28**, 3177 (1985).

[20]H. Motz, *J. Appl. Phys.* **22**, 527 (1951).

[21]M. Phillips. *IRE Trans. Elect. Dev.* **ED-7**, 231 (1960).

Figure Captions

Fig. 1. Schematic of the free-electron laser.

Fig. 2. Typical oscilloscope trace of (a) the beam voltage and (b) the microwave output signal. 1 marks the amplitude of the 8.2GHz CW injected signal; 2 marks the amplified slow space charge wave FEL signal; 3 marks the damped fast space charge wave FEL signal.

Fig. 3. Microwave power output as a function of power input for two different values of wiggler amplitude B_w. The solid line is from small signal theory (see text) which does not allow for saturation effects obseved at high input power.

Fig. 4. Gain as a function of the wiggler field amplitude B_w. The solid line is from three-dimensional theory.

Fig. 5. The gain G and the growth rate factor Γz as a function of axial distance z within the wiggler. The points and squares are from experiment with B_w = 146G; $B_{||}$ = 1512G; I = 4.4A; f = 10.6GHz. The lines are from theory.

Fig. 6. The gain as a function of frequency for two different wiggler strengths B_w. The solid lines are from theory.

Fig. 7. The gain G and the normalized growth rate $\Gamma/I^{1/4}$ as a function of beam current I. The points are from experiment with B_w = 170G and $B_{||}$ = 1580G. The solid lines are from cold beam, Raman theory. The dashed lines are from warm beam theory (see text).

Fig. 8. The normalized growth rate $\Gamma/I^{1/4}$ as a function of axial magnetic field, illustrating growth enhancement near resonance $\Omega_{||} \approx k_w \beta_{||} c$; B_w = 122G, I = 3.5A, f = 9.25GHz. The solid line is from theory.

Fig. 9. Ratio of the output power in the orthogonal polarization, to the

output power in the incident polarization, as a function of the wiggler amplitude B_w for $B_{||} = 1580$G and $I \approx 5.7$A. The lines are from theory.

Fig. 10. The ratio of the output power to the input power for the fast space charge wave interaction. Measurements for the incident polarization are given by the dots, and for the orthogonal polarization by the crosses; $B_{||} = 1422$G; $I \approx 2.4$A; $f = 10.4$GHz. The line is from theory.

Fig. 11. The gain and relative phase shift as a function of beam voltage. The solid lines are from experiment, the dashed lines are from theory; $B_w = 122$G; $B_{||} = 1512$G; $I = 3.5$A; $f = 11.1$GHz.

Fig. 12. The gain and relative phase shifts as a function of beam voltage. The solid lines are from experiment, and the dashed lines from theory. (a) through (d) represent different regions of FEL operation (see section VII) $B_{||} = 1312$G; $f = 10.4$GHz.

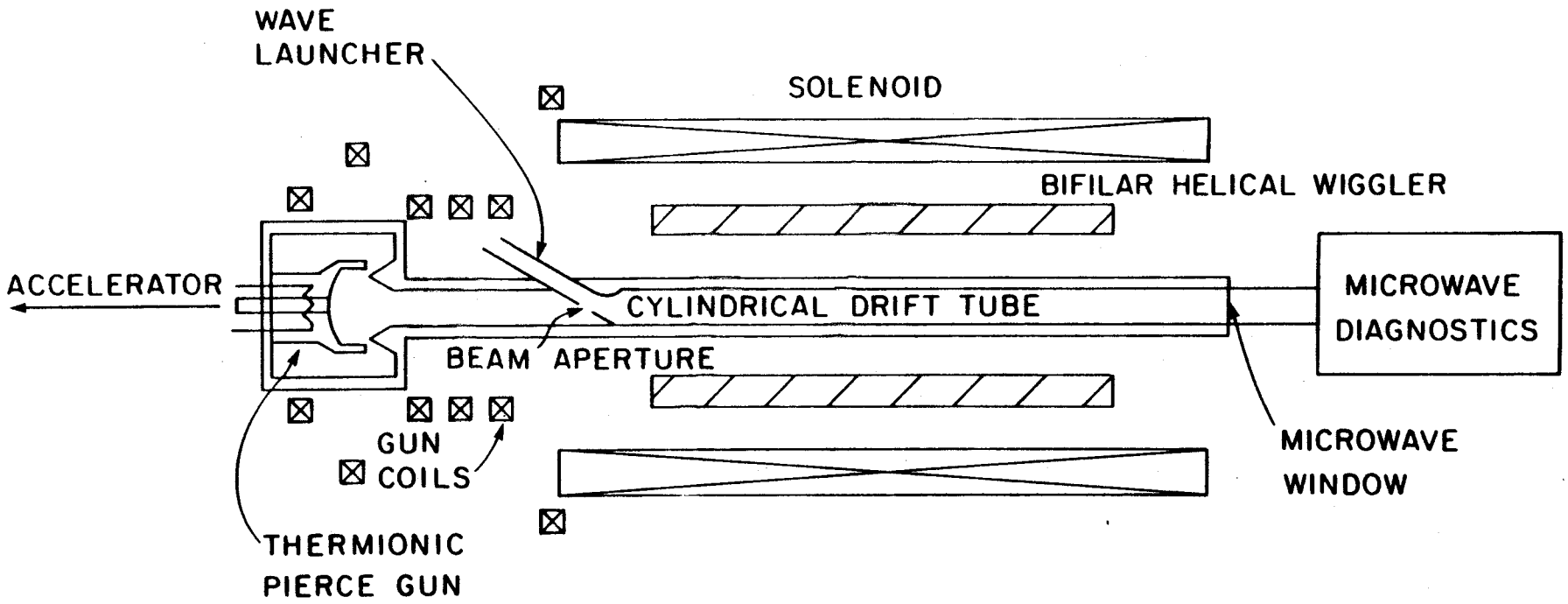

Fig. 1
Fajans & Bekefi

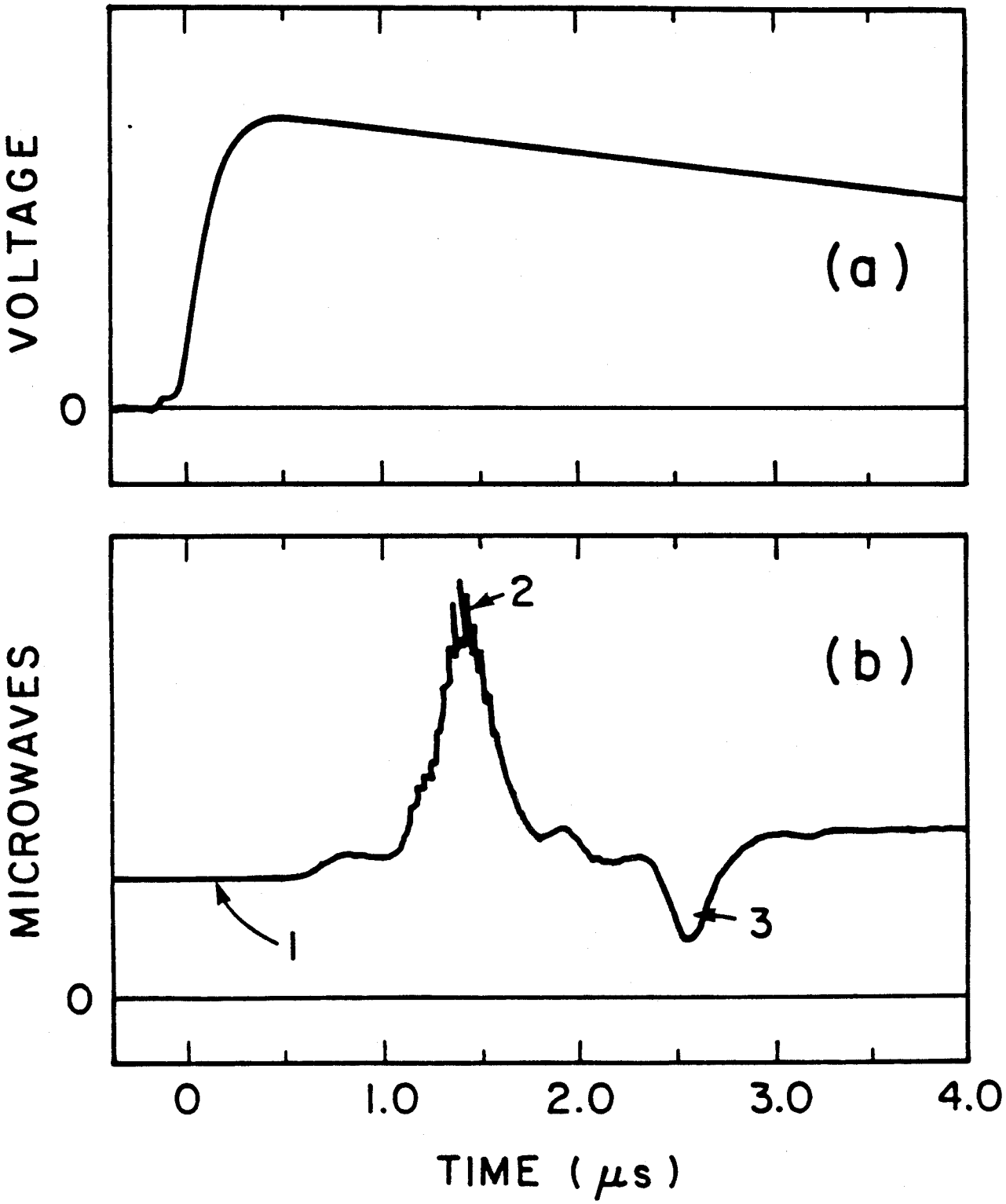

Fig. 2
Fajans & Bekefi

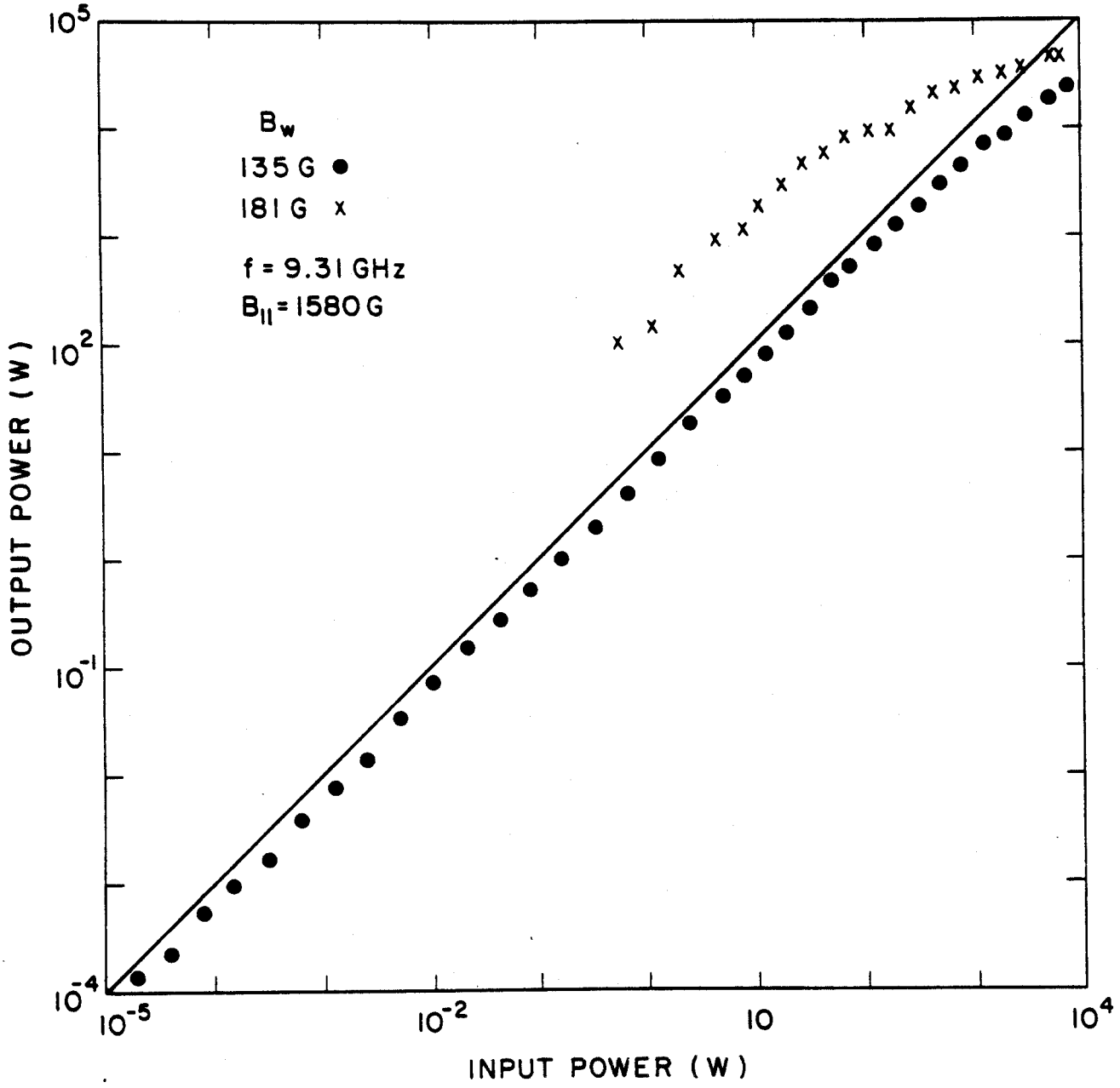

Fig. 3
Fajans & Bekefi

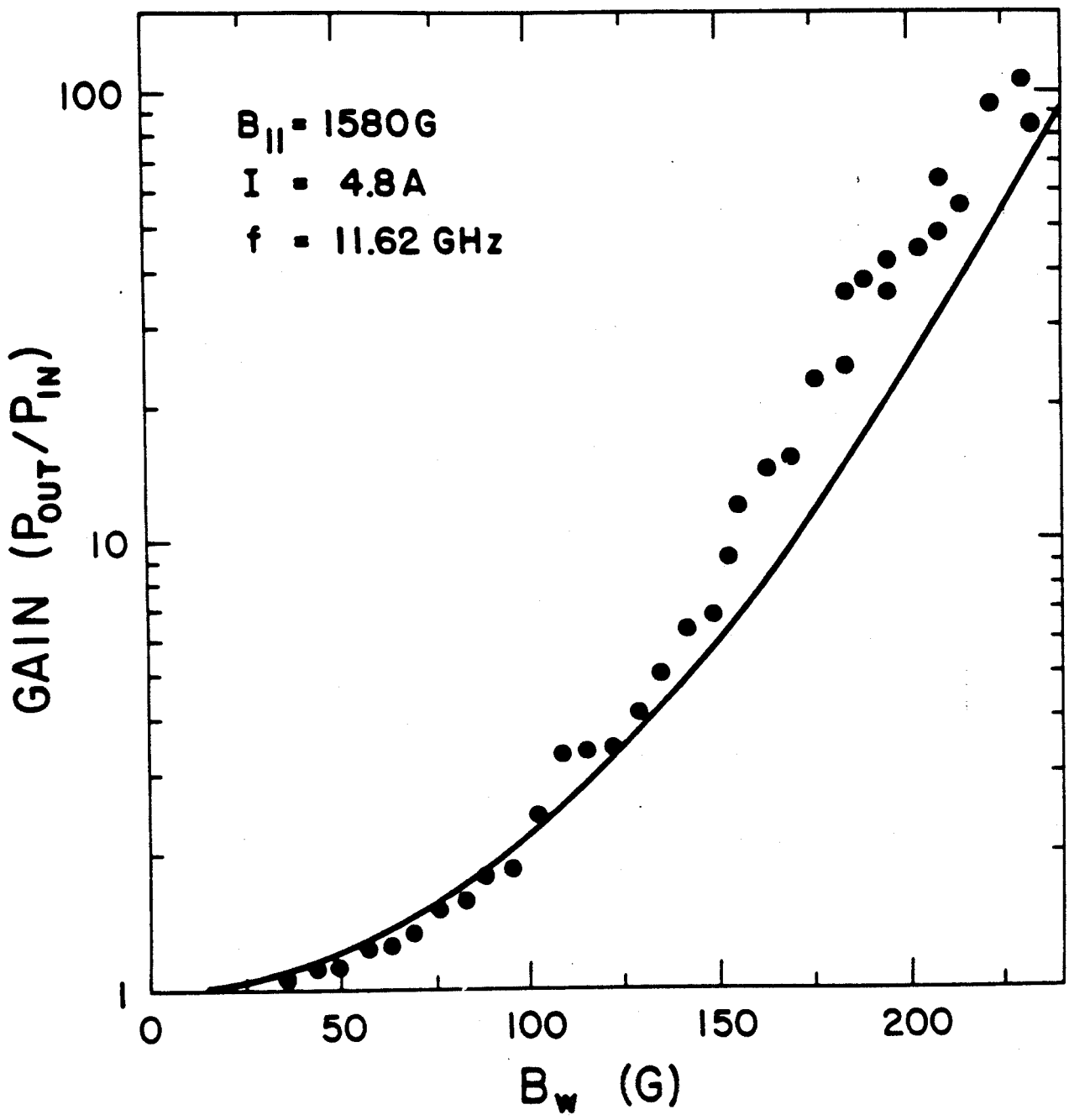

Fig. 4
Fajans & Bekefi

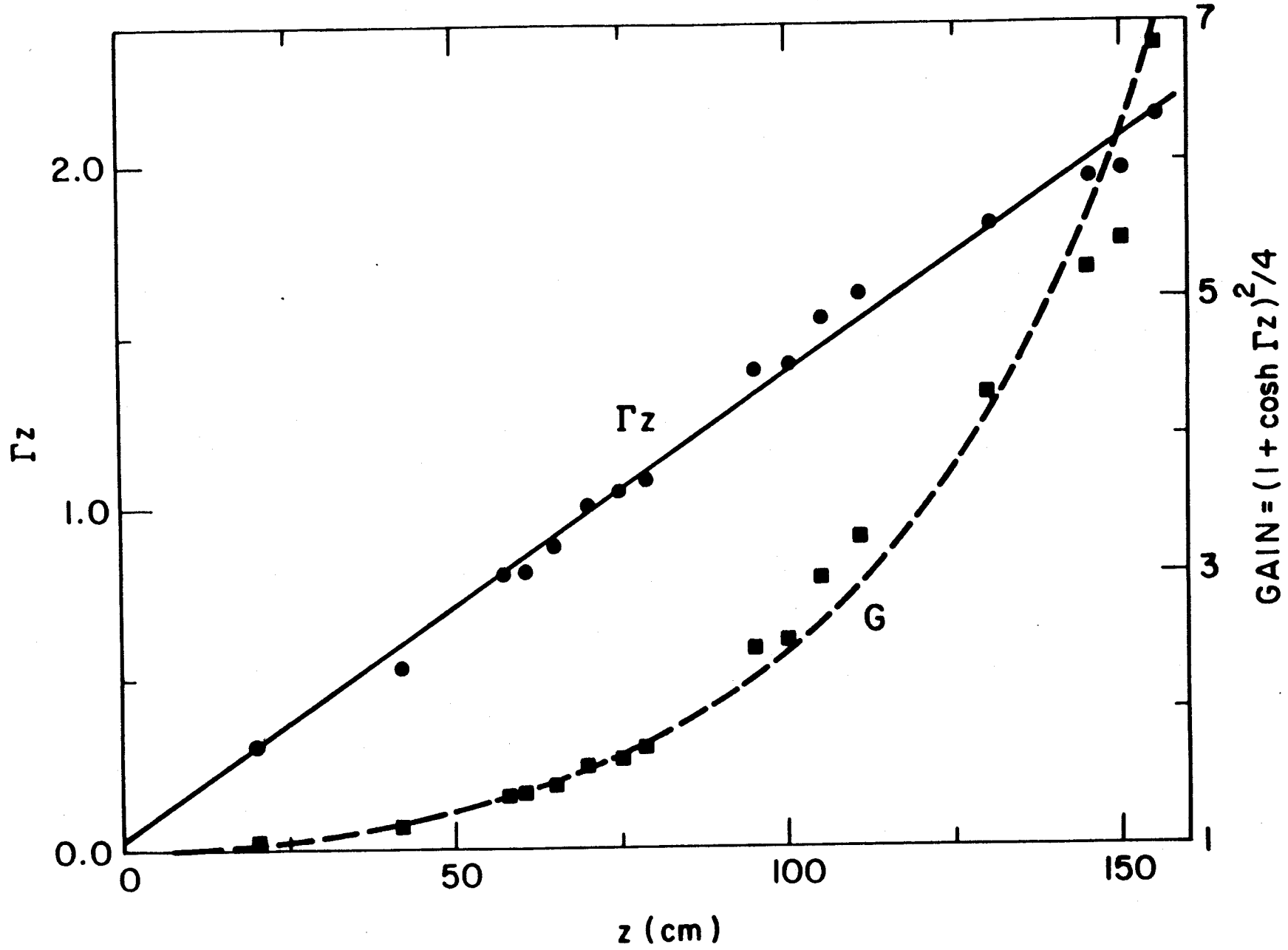

Fig. 5
Fajans & Bekefi

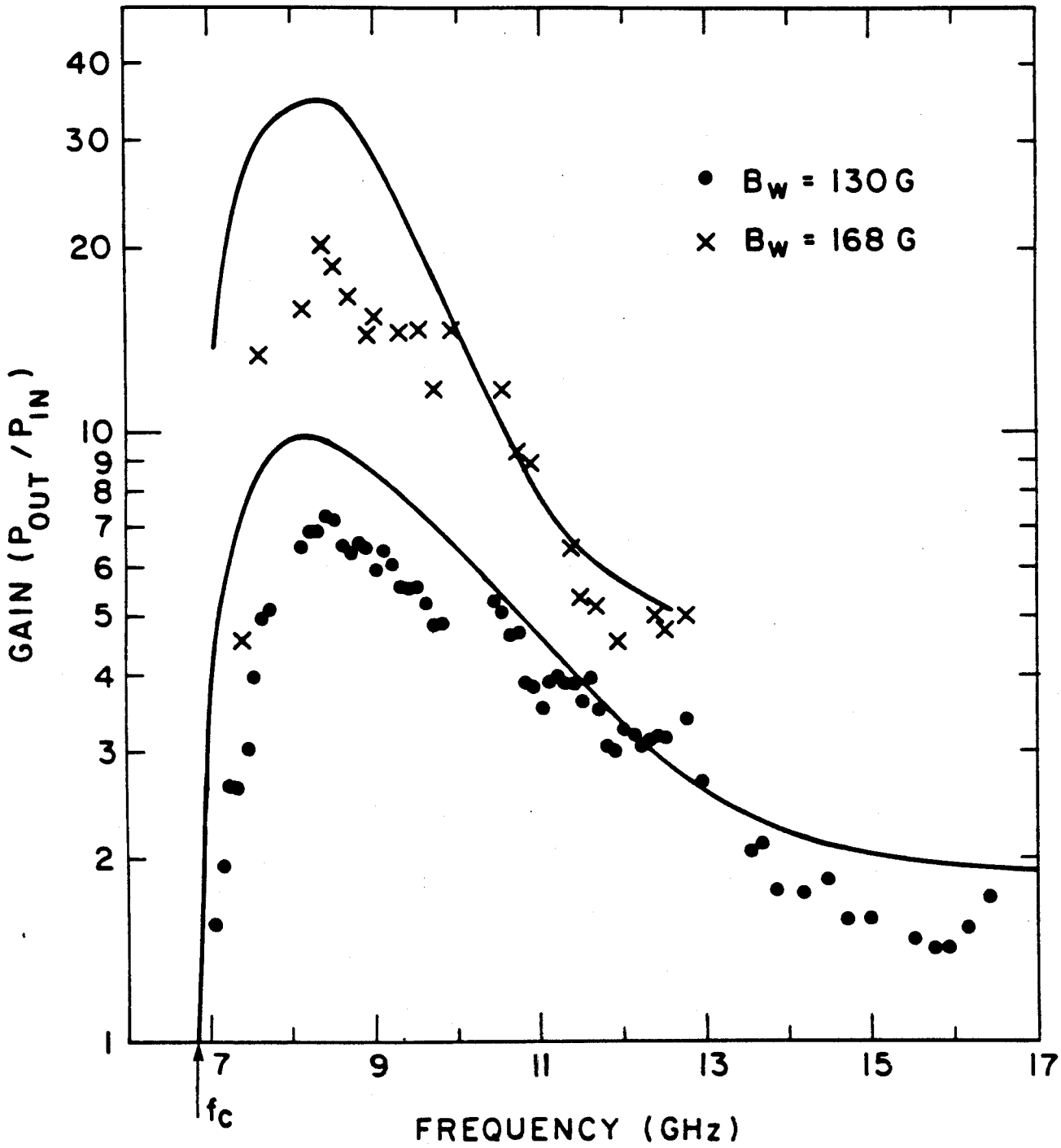

Fig. 6
Fajans & Bekefi

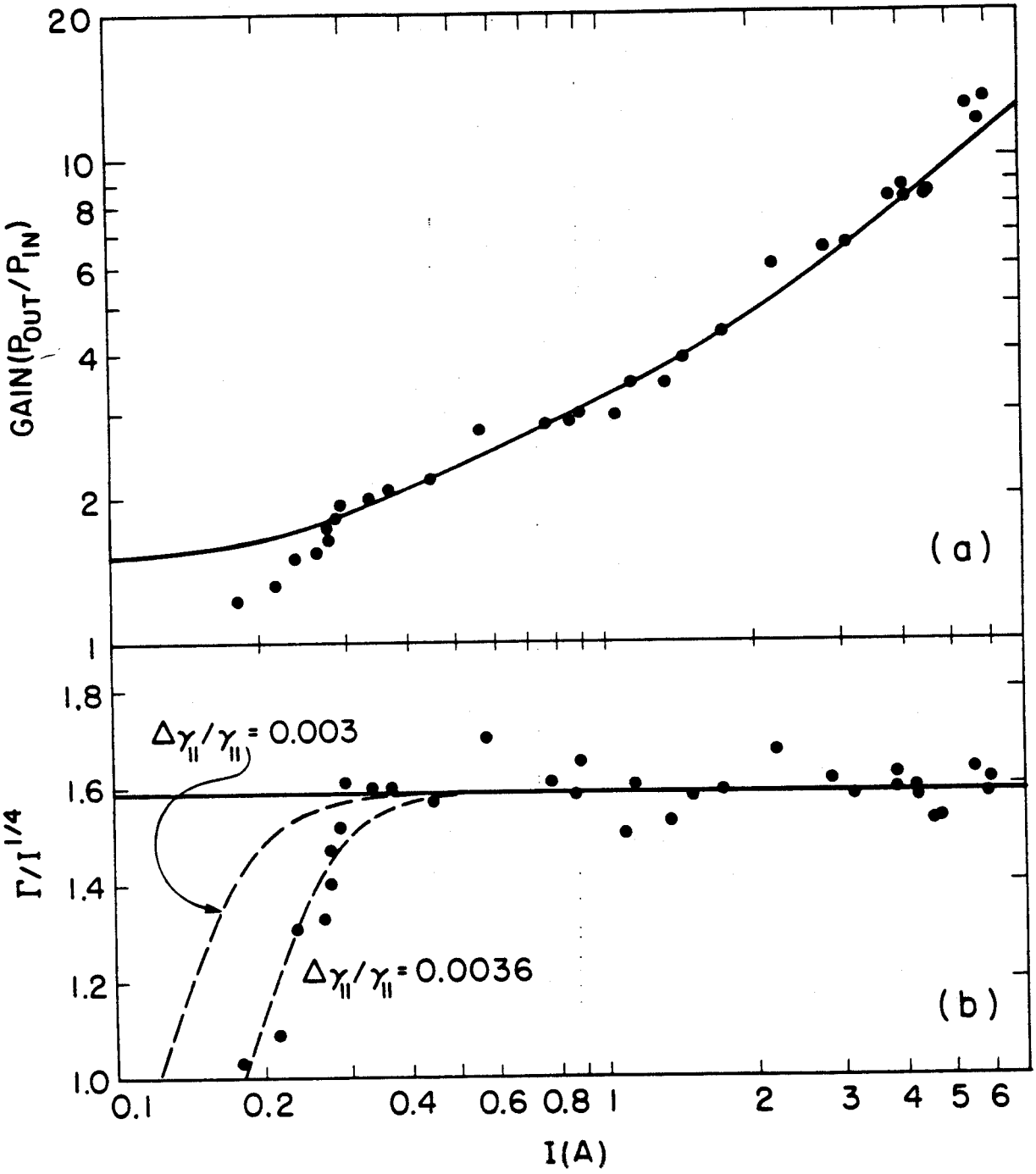

Fig. 7
Fajans & Bekefi

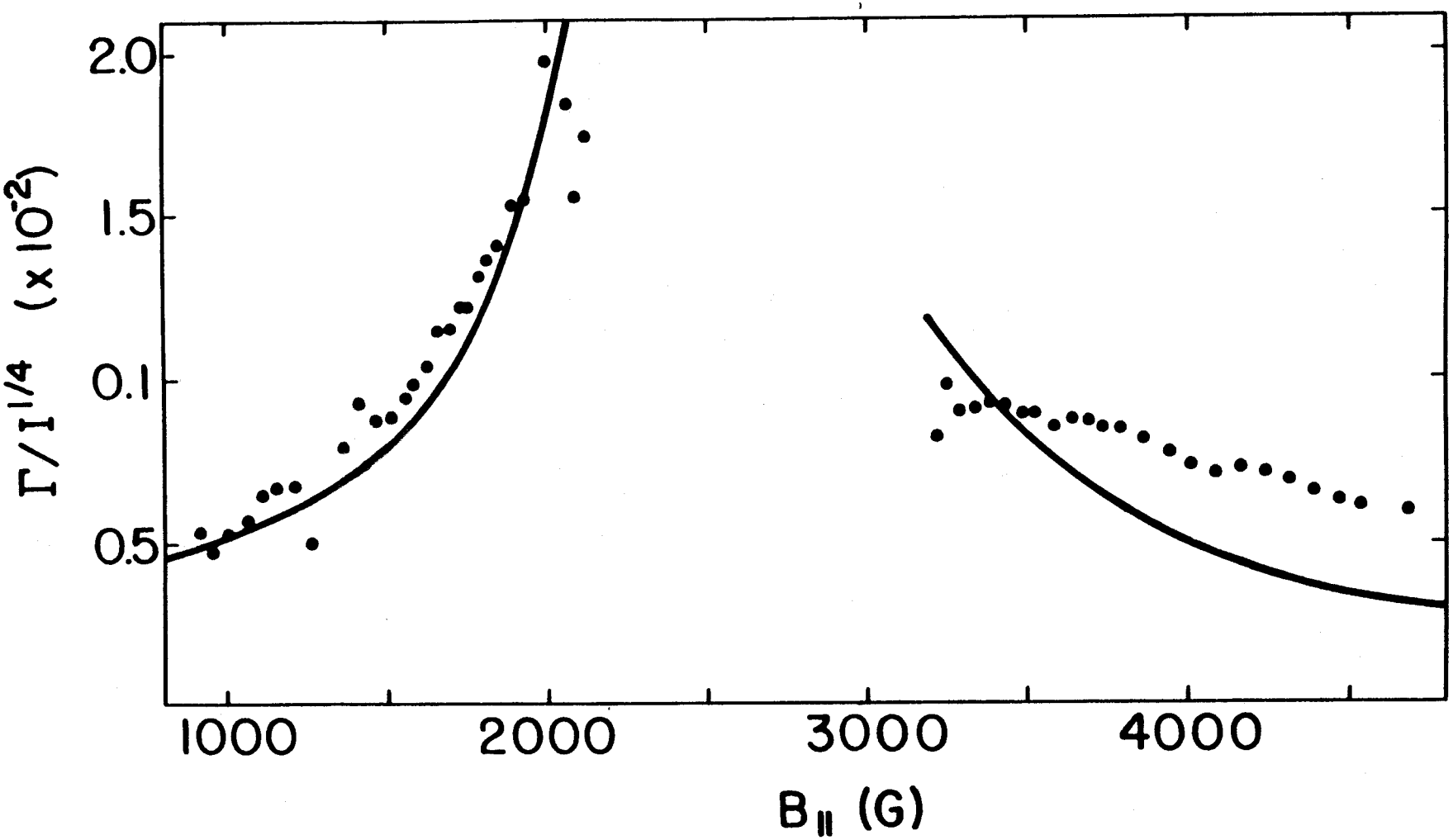

Fig. 8
Fajans & Bekefi

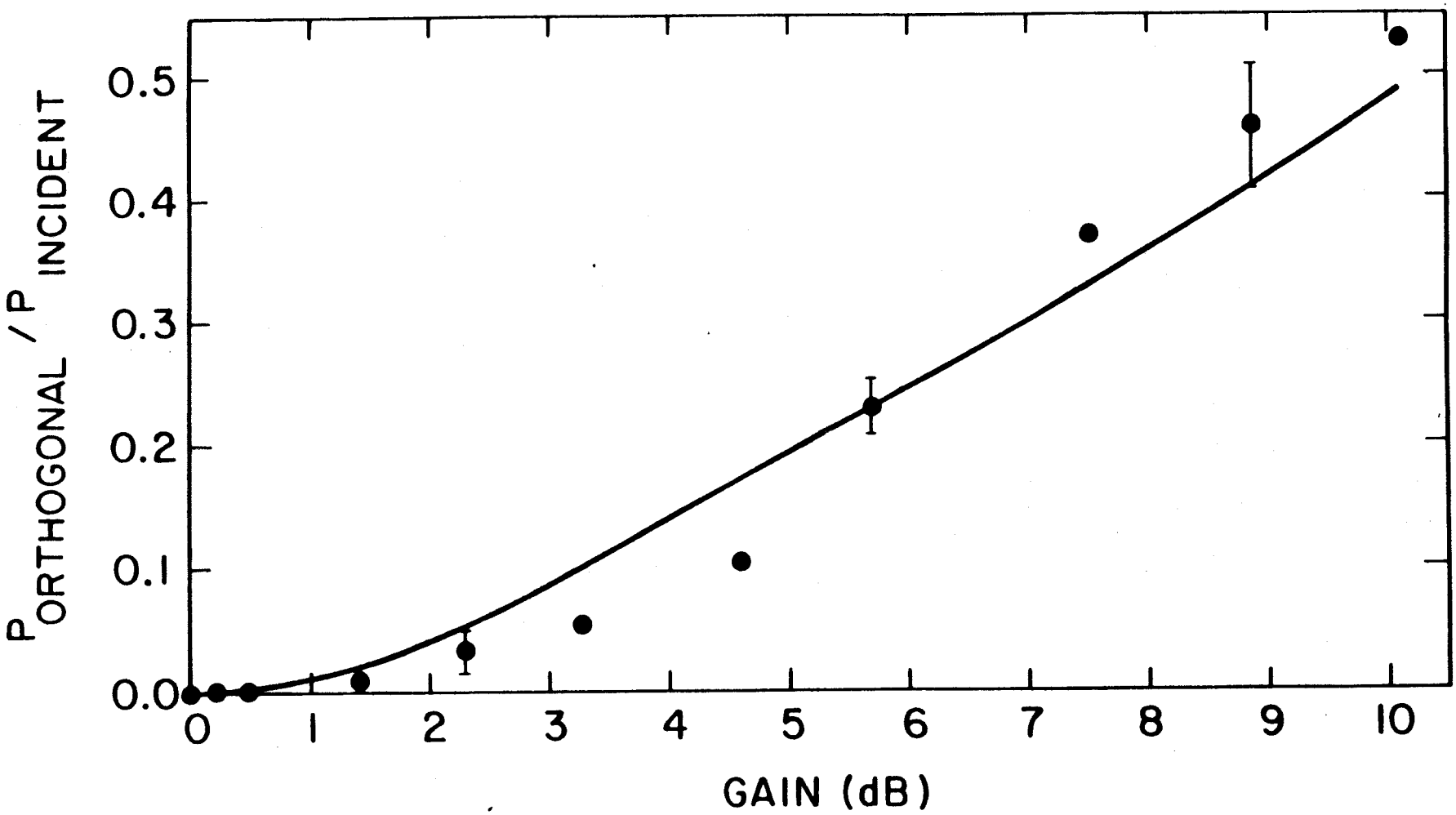

Fig. 9
Fajans & Bekefi

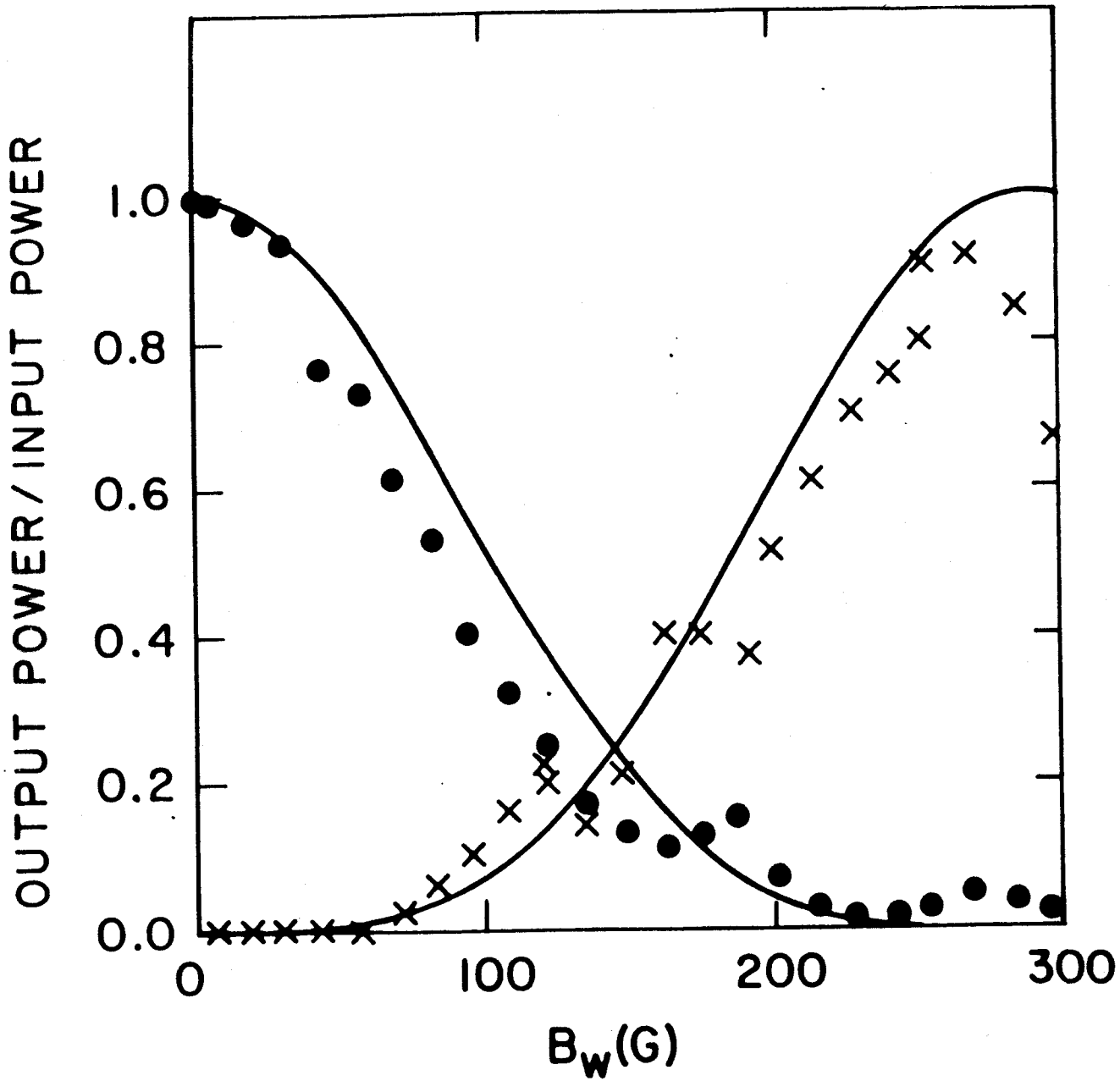

Fig. 10
Fajans & Bekefi

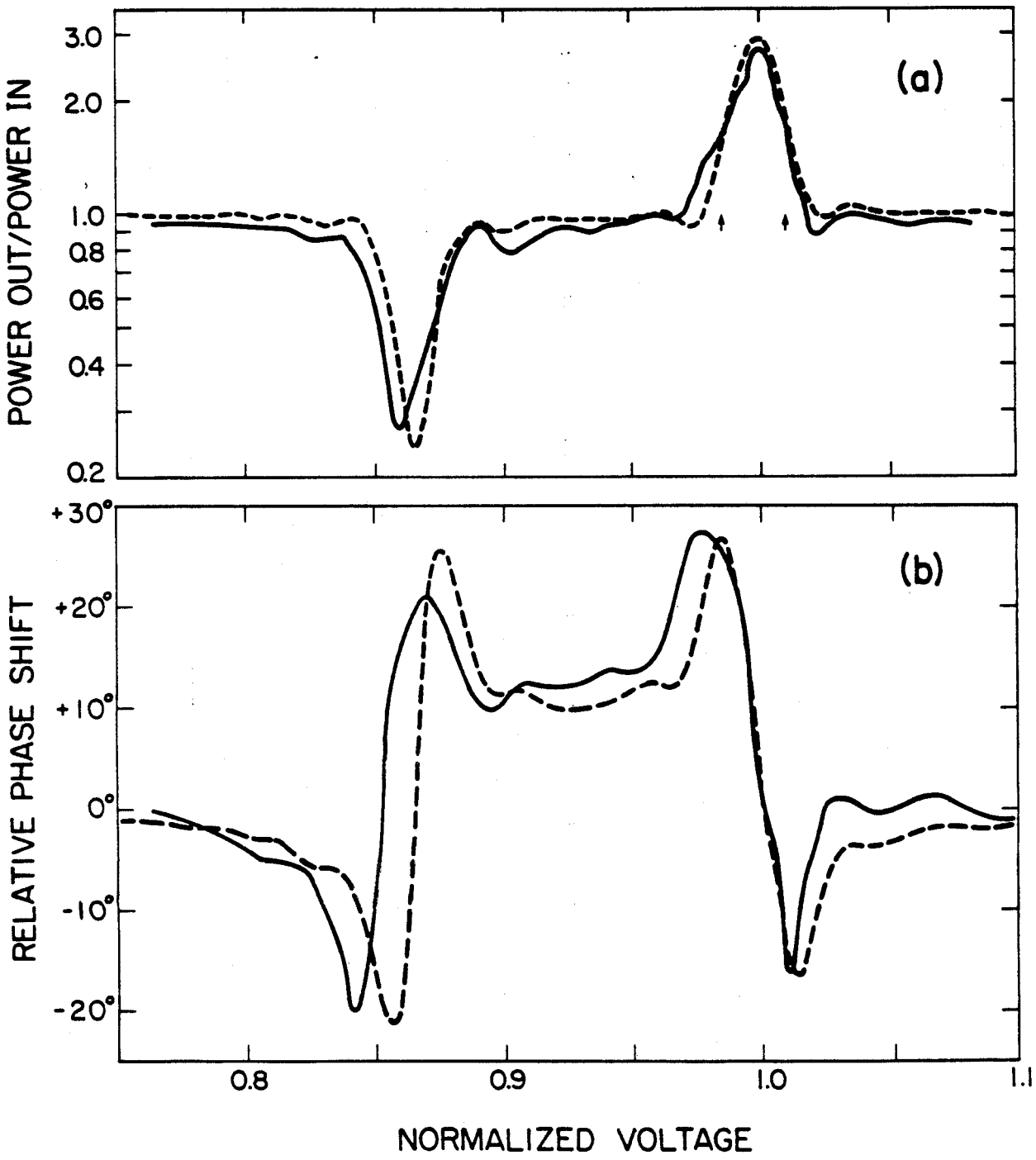

Fig. 11
Fajans & Bekefi

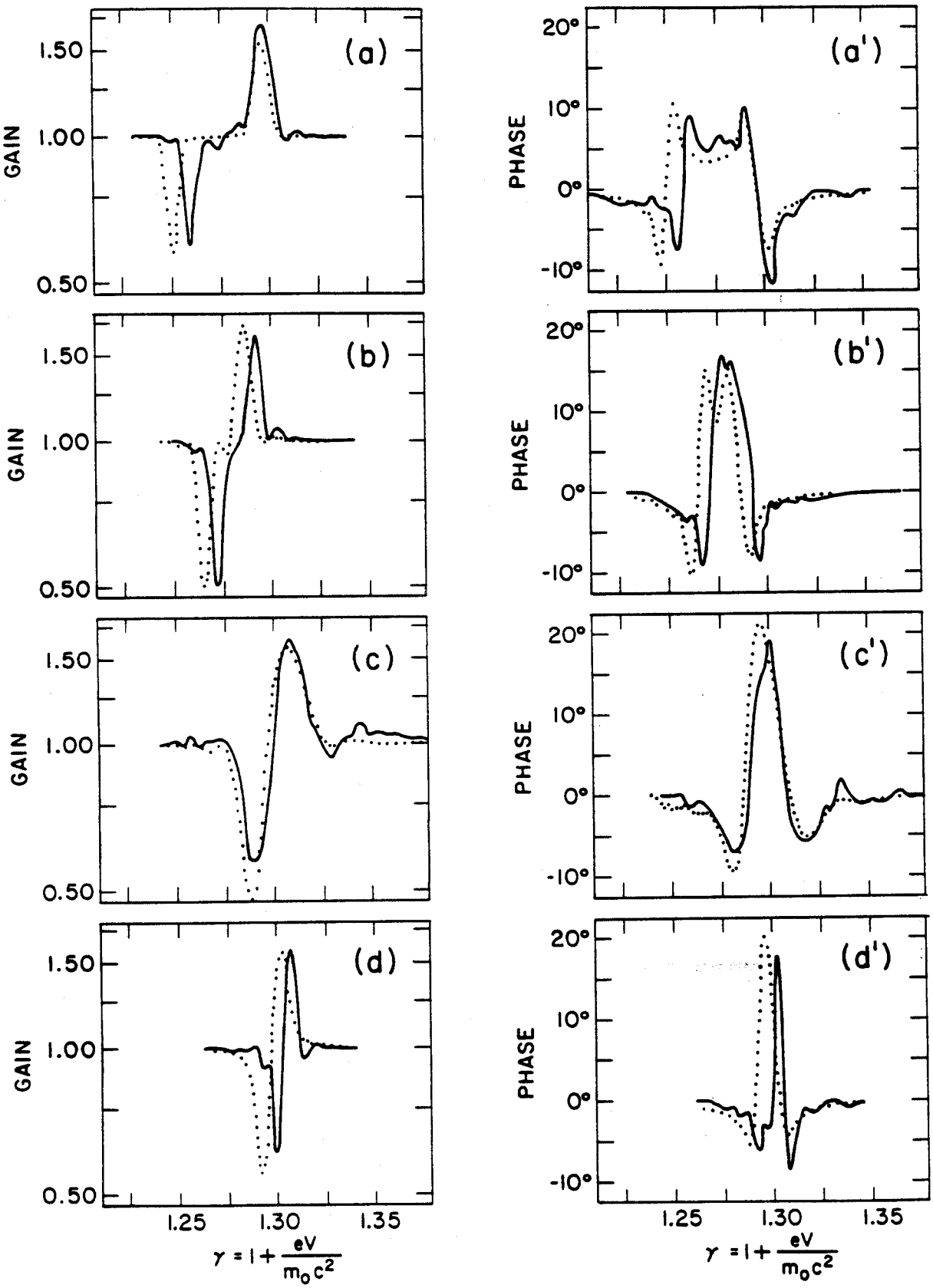

Fig. 12
Fajans & Bekefi